MODELING OF A FLOWING Ar-O$_2$ MICROWAVE DISCHARGE AND POST-DISCHARGE

K. KUTASI[1,2], V. GUERRA[1], P. A. SÁ[1,3] and J. LOUREIRO[1]

[1] *Instituto de Plasmas e Fusão Nuclear, Instituto Superior Técnico,*
1049-001 Lisboa, Portugal

[2] *Research Institute for Solid State Physics and Optics, Hungarian Academy of Sciences,*
POB 49, H-1525 Budapest, Hungary
E–mail: kutasi@sunserv.kfki.hu

[3] *Departamento de Eng.Fízica, Faculdade de Engenharia da Universidade do Porto,*
4200-465 Porto, Portugal

Abstract. A flowing Ar-O$_2$ microwave discharge and its afterglow have been investigated by means of a 1-D kinetic and a 3-D hydrodynamic model, respectively. The evolution of the densities of species created in the discharge have been determined along the early afterglow present in the connecting tube between the discharge region and reactor, as well as in the late afterglow developed in a large reactor.

1. INTRODUCTION

Ar-O$_2$ plasmas are widely used in material processing and biomedical applications, e.g. the post-discharge of Ar-O$_2$ has been successfully used as oxidizing media in deposition of oxide films (Belmonte et al. 1997), and the inactivation of bacterial spores have been achieved in the flowing afterglow of an Ar-O$_2$ microwave discharge (Moreau et al. 2000). In pure Ar post-discharges the main sterilizing agents are believed to be the VUV photons (105-107 nm) emitted by the Ar atoms in the resonant states, whereas in Ar-O$_2$ mixture the VUV photons and O atoms. The aim of this work is to follow by modeling the evolution of the densities of active species produced by a flowing Ar-O$_2$ microwave discharge, from the discharge region to the late-afterglow present in a large volume reactor, thus contributing to the understanding of the elementary processes occurring in these systems, in particular those responsible for plasma sterilization.

2. MODELING

Figure 1 shows the post-discharge system set-up used in our investigations, similar to the one used in (Pintassilgo et al. 2007). The discharge is generated in a 0.8 cm diameter silica tube, which is connected with a 2.6 cm diameter tube to a $60 \times 30 \times 28$ cm^3 reactor made of aluminum. The gas inlet and outlet are symmetrically positioned in the middle of the left side and bottom walls, respectively.
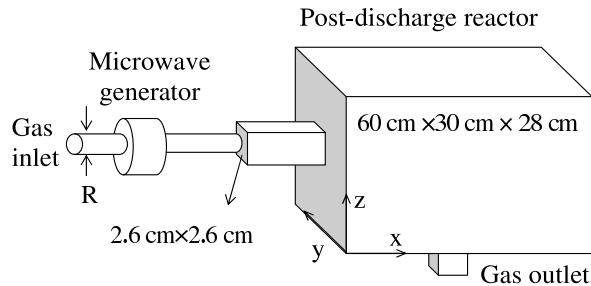
Figure 1: The post-discharge system set-up.

The system is described with two different models valid for the discharge and early afterglow region, and for the late afterglow present in the large reactor, respectively. The species densities in the discharge region are calculated by solving the homogeneous electron Boltzmann equation, coupled together with the rate balance equations describing the creation and destruction of $Ar(^1S_0, {}^3P_2, {}^3P_1, {}^3P_0, {}^1P_1)$, $O_2(X^3\Sigma_g^-,v)$, $O_2(a^1\Delta_g, b^1\Sigma_g^+)$, $O(^3P)$, O_3, Ar^+, O_2^+, O^+, O^-, under the assumption of a quasi-neutral discharge. The concentrations obtained for the steady-state discharge are used as initial values to the early afterglow taking place in the tube connecting the discharge to the main reactor, where the same system of equations is solved in time under zero electric filed. The evolution of the species densities in the post-discharge reactor are followed with a 3-D hydrodynamic model (Kutasi et al. 2007), where only the neutral active species are considered.

3. RESULTS AND DISCUSSION

The discharge results have been obtained at f=2.45 GHz, p=400 Pa, T_g=1000 K, in a 99%Ar-1%O$_2$ mixture with electron density n_e=3.74×10^{11} cm^{-3}, which is the critical value for surface-wave propagation. In the early afterglow the gas temperature is assumed to be 500 K. The gas flow rate is 500 sccm, while the flight time of species in the connecting tube between the discharge and reactor is assumed to be 10^{-4}s.

Figure 2 shows the time evolution of several species in the early-afterglow. As it is clearly seen, the Ar(4s) states are quickly depleted. As a matter of fact, they are very effectively quenched by O atoms in Ar(4s)+O→ Ar($^1S_0$)+O process and O$_2$ molecules through the Ar(4s)+O$_2$→ Ar($^1S_0$)+O+O reaction. Another relevant point is that O$_2$ is strongly dissociated, both by electron impact with O$_2$(X,a,b) and by Ar(4s) atoms. The latter contributes about 15% to the total dissociation rate.

The results of the hydrodynamic model show that the Ar metastable and resonant states become totally depopulated in the vicinity of the reactor's entrance. These results suggest that, contrary to the earlier suppositions (Moreau et al. 2000), the Ar resonant states cannot contribute to the VUV/UV emission in the reactor. Figure 3 shows the relative density distribution of O atoms in the central (y = 15 cm) x-z vertical plane of the reactor (the gas enters the reactor in the z = 12-14.6 cm region). According to this, the O atoms density decreases from the entrance towards the walls about one order of magnitude. The loss of O atoms in the reactor is due to their surface recombination, the loss probability for the aluminum surface has
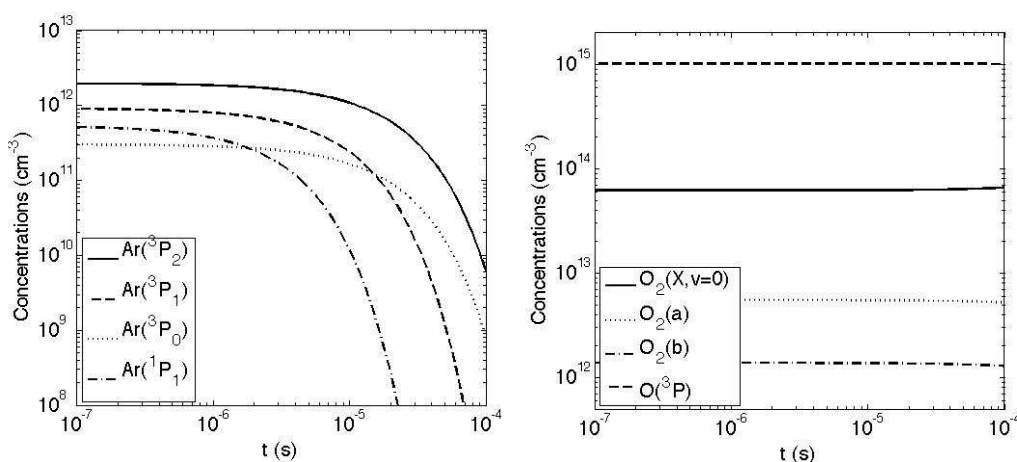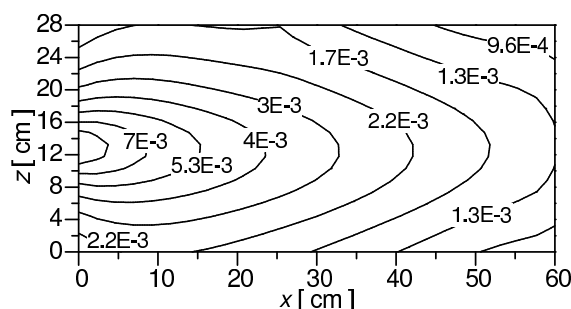
352

Figure 2: Time evolution of heavy-particles along the early afterglow.

Figure 3: The relative density of O atoms in the reactor for x-z vertical plane at $y=$ 15 cm.

been chosen $\gamma_O=1.7\times10^{-3}$ (Wickramanayaka et al. 1991). A more homogeneous density distribution, which is more favorable for applications, can be achieved in Pyrex reactors, where the atomic recombination on the surface is less efficient.

Figure 4 shows the relative density distribution of $O_2(a)$ and $O_2(b)$ in the central ($y = 15$ cm) x-z vertical plane of the reactor. The density of $O_2(a)$ decreases about one order of magnitude in the reactor from the entrance to the walls, while the $O_2(b)$ density two orders of magnitude. In case of $O_2(a)$, similarly to the $O(^3P)$ atoms, the losses are mainly due to the surface recombination, while in the case of $O_2(b)$ besides the surface recombination the quenching by $O(^3P)$ has also a great contribution. The surface loss probabilities of $O_2(a)$ and $O_2(b)$ have been taken $\gamma_{O2(a,b)}=1\times10^{-3}$ from (Sharpless et al. 1989).

The evolution of the species for different discharge conditions, especially gas mixture composition, which influence the dissociation degree of the O_2 molecules and also the quenching of radiative Ar states, are investigated and will be presented at the meeting. The influence on the UV radiation of N_2 impurities, which can be present in the system, will be discussed as well.
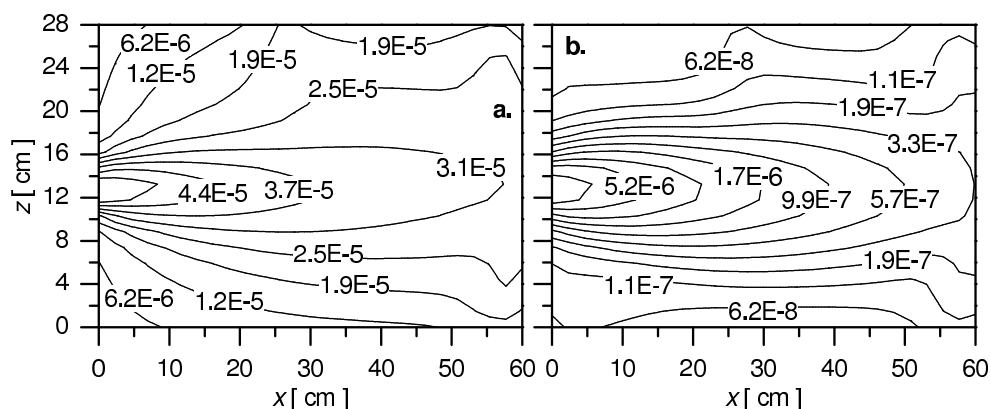
Figure 4: The relative density of a) $O_2(a)$ and b) $O_2(b)$ molecules in the reactor for x-z vertical plane at y= 15 cm.

Acknowledgments

References

Belmonte, T. et al.: 1997, *Surf. Coat. Technol.*, **97**, 642.

Kutasi, K., Loureiro, J.: 2007 *J. Phys. D: Appl. Phys.*, **40**, 5612.

Moreau, S. et al.: 2000 *J. Appl. Phys.*, **88**, 1166.

Pintassilgo, C. D., Kutasi, K., Loureiro, J.: 2007 *Plasma Sources Sci. and Technol.*, **16**, S115.

Sharpless, R. L. and Slanger T. G.: 1989 *J. Chem. Phys.*, **91**, 7947.

Wickramanayaka, S., Meikle, S., Kobayashi, T., Hosokawa, N., Hanataka, Y.: 1991 *J Vac. Sci. Technol A*, **9**, 2999.